




# SFMambaNet: Spectral-Frequency Enhanced Selective State Space Model for Correspondence Pruning

Zhihua Wang , Yanping Li , Yizhang Liu 

**Abstract**—Correspondence pruning aims to identify inliers from an initial set of correspondences. Most existing Graph Neural Network (GNN)-based methods rely on geometric features mapped from coarse Euclidean coordinates, which struggle to capture the subtle geometric consistencies presented by inliers. While Mamba-based methods possess global receptive fields and long sequence modeling capabilities, they tend to accumulate substantial inconsistent features within the hidden state space, making it difficult to distinguish inliers from outliers. In this paper, we integrate frequency domain perception into this task for the first time and propose SFMambaNet, a novel Spectral-Frequency enhanced Mamba-based two-view correspondence pruning network. Our method is collaboratively composed of two components: First, we design a Local Spectral-Geometric Attention (LSGA) block. LSGA incorporates spectral positional encoding into local graph interactions and introduces multi-scale Mamba processing to enhance the capture of subtle geometric consistencies and improve local feature discriminability. Building upon this, we design a Spectral-Integrated Global Mamba (SIGM) block. SIGM embeds a frequency gating mechanism within the state space, utilizing the frequency information provided by LSGA to explicitly suppress high-frequency noise accumulation within hidden states and mitigate the propagation of inconsistent features. This enhances inlier-outlier separability and achieves robust global context modeling capabilities with nearly linear complexity. Extensive experiments demonstrate that SFMambaNet outperforms current state-of-the-art methods on several challenging tasks. The code is available at <https://github.com/Kirito14IT/SFMambaNet>.

**Index Terms**—Correspondence pruning, Spectral-Frequency Domain, Selective State Space model, Graph Neural Networks, Transformer.

## I. INTRODUCTION

**E**STABLISHING reliable and accurate correspondences between image pairs serves as a fundamental prerequisite for a myriad of computer vision tasks. These distinctive feature matches act as the cornerstone for downstream applications, ranging from visual localization [1] and image registration [2], [3] to more complex systems like simultaneous localization and mapping (SLAM) [4], structure from motion (SfM) [5], and point cloud registration [6]. Typically, the correspondence learning pipeline begins with detecting and describing local features using handcrafted detectors like SIFT [7] or learning-based extractors such as SuperPoint [8]. While these methods

Zhihua Wang is with the School of Optical-Electrical and Computer Engineering, University of Shanghai for Science and Technology, Shanghai 200093, China (e-mail: wzh2657751462@gmail.com).

Yanping Li is with the Institute of Artificial Intelligence, Shanghai Jiao Tong University, Shanghai, China (e-mail: ypli2024@sjtu.edu.cn).

Yizhang Liu is with the College of Computer and Data Science/College of Software, Fuzhou University, Fuzhou 350108, China (e-mail: lyz8023lyp@gmail.com).

Corresponding author: Yizhang Liu.

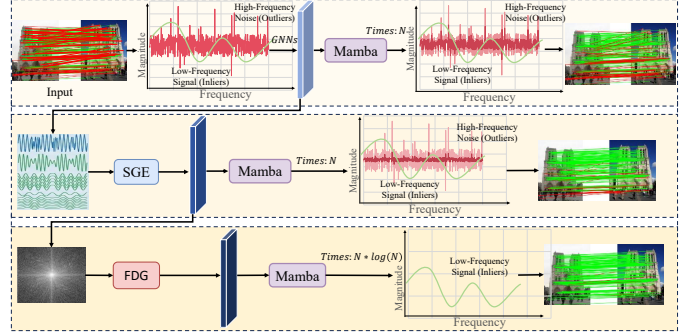


Fig. 1. Visual comparison in the spatial and frequency domains under three configurations, where the first configuration operates solely in the spatial domain, and the latter two introduce frequency-domain perception: GNNs with Mamba, SGE with Mamba, and SGE with FDG and Mamba. **SGE**: Spectral-Geometric Encoding operation. **FDG**: Frequency-domain gating operation.

perform well in standard scenarios, they inevitably generate a set of putative correspondences contaminated by a significant ratio of outliers. This degradation is particularly severe in challenging environments characterized by extreme viewpoint changes, repetitive textures, or varying illumination conditions. Consequently, filtering out these mismatches (outliers) to preserve only the correct ones (inliers) is imperative for ensuring the precision of camera pose estimation and other geometric tasks.

Over the past decades, correspondence pruning algorithms can be broadly categorized into traditional heuristic strategies and learning-based approaches. Classic robust estimators, represented by RANSAC [9] and its variants [10], rely on iterative hypothesis generation and verification to fit geometric models. Although widely adopted, their required number of hypotheses grows exponentially with the outlier ratio, making them computationally expensive when the inlier ratio is low [11]. To transcend these limitations, LFGC [12] pioneered the integration of deep neural networks into this field, reformulating correspondence pruning as a binary classification problem. This shift has inspired a surge of data oriented solutions that leverage spatial context to achieve superior robustness. In recent years, Transformer-based methods, such as VSFormer [13] and TransMatch [14], were introduced to model global contexts through self-attention mechanisms. While the attention mechanism is critical to the effectiveness of Transformers, its computational complexity grows quadratically with sequence length. Subsequently, works based on Graph Neural Networks (GNNs) have achieved remarkable success in modeling geometric contexts. Early works like NMNet [15] and CLNet [16] utilized GNNs to capture local topological structures via message passing. NCMNet [17]

defines a local message passing mechanism and propagates information by stacking multiple layers. However, most of the above methods solely rely on geometric features mapped from coarse Euclidean coordinates, which significantly limits their ability to capture the subtle geometric consistencies inherent to inliers.

Mamba [18] advances the Structured State Space Sequence Model (S4) [19] to address the limitations of discrete data modeling. By offering a global receptive field with linear complexity distinct from Convolutional Neural Networks (CNNs) and Transformers, Mamba has inspired improvements in correspondence pruning such as MatchMamba [20]. Although Mamba excels at long-range modeling, these works often overlook the necessity of possessing both full spatial perception and frequency perception simultaneously, thereby limiting the model’s robustness against complex deformations [21]. More critically, the standard scanning mechanism treats correspondences as flattened sequences, resulting in the accumulation of a large amount of inconsistent features within the hidden state space due to the lack of explicit frequency perception. In the context of two-view correspondence learning, true correspondences (inliers) typically share smooth, consensus-driven geometric transformations, manifesting as stable, low-frequency signals [22]. Conversely, false correspondences (outliers) exhibit random, structurally chaotic spatial variations, inherently acting as erratic high-frequency noise [22], [23]. However, the structural rigidity of standard state space models prevents the effective decoupling of such high-frequency noise from low-frequency geometric signals during sequential state transitions. Consequently, this directly dilutes the consistency of global geometric features, making it difficult to distinguish inliers from outliers.

To address the above challenges, we propose SFMambaNet, a spectral-frequency enhanced Mamba-based network for correspondence pruning. Instead of relying on a single notion of frequency perception, SFMambaNet introduces frequency modeling at two complementary levels. First, in the local modeling stage, we design a Local Spectral-Geometric Attention (LSGA) block, which performs spectral expansion over relative neighborhood coordinates to enrich the representation of fine-grained geometric variations. By embedding spectral positional encoding into local graph interactions, LSGA enhances the discriminability of subtle geometric consistencies that are difficult to preserve in the original low-dimensional Euclidean space. Second, in the global modeling stage, we develop a Spectral-Integrated Global Mamba (SIGM) block, which performs learnable spectral filtering over the propagated feature sequence. Specifically, SIGM incorporates a frequency gating mechanism into the Mamba state space to attenuate rapidly varying and unstable feature components during long-range state transitions, thereby improving global consensus modeling. In this way, LSGA emphasizes local geometric frequency modeling, whereas SIGM focuses on global sequence-level spectral filtering; the two modules work jointly to improve both local discriminability and global consistency for correspondence pruning (as illustrated in Fig. 1).

In summary, the contributions of this work are as follows:

- **We propose a Local Spectral-Geometric Attention**

**(LSGA) block for fine-grained local correspondence modeling.** By introducing spectral positional encoding over relative coordinates into local graph interactions, LSGA enhances the representation of subtle geometric variations and improves the discrimination of geometrically consistent correspondences. In addition, a spectral-spatial cluster Mamba is incorporated to further strengthen local geometric context aggregation.

- **We propose a Spectral-Integrated Global Mamba (SIGM) block for robust global context modeling.** Different from LSGA, SIGM operates on the propagated feature sequence and introduces a learnable frequency gating mechanism into the Mamba state space, which suppresses unstable oscillatory components during long-range state transitions and mitigates the accumulation of inconsistent features, while maintaining favorable computational efficiency.
- **Finally, we present SFMambaNet, the first spectral-frequency enhanced State Space Model that integrates frequency domain perception into the correspondence pruning task.** Extensive experimental results demonstrate that SFMambaNet outperforms current state-of-the-art methods on tasks such as camera pose estimation and outlier rejection with highly competitive efficiency.

The paper is organized into five main sections. Section II surveys the related work. The architectural methodology of SFMambaNet is detailed in Section III, followed by a comprehensive experimental analysis in Section IV. Concluding remarks are presented in Section V.

## II. RELATED WORK

### A. Traditional Correspondence Pruning

Traditional methods for correspondence pruning generally fall into two groups: heuristic resampling methods and spatial constraint-based methods. RANSAC [9] is the most representative resampling method. It works by randomly selecting data subsets to fit a geometric model iteratively. To improve efficiency, its variants have been proposed. For instance, PROSAC [24] accelerates the search process by prioritizing matches with higher similarity scores. MAGSAC [25] introduces a marginalization strategy to remove the dependence on manually set thresholds. While these methods are robust, they often become computationally expensive when the outlier ratio is high. Spatial constraint-based methods focus on exploring spatial constraints among correspondences. VFC [26] assumes that correct matches form a smooth motion field and uses Tikhonov regularization to filter outliers. GMS [23] incorporates motion smoothness into grid-based statistics to distinguish inliers. Similarly, LPM [27] identifies true matches by preserving the local neighborhood structure of points. Although these methods are faster than RANSAC-based approaches, their performance tends to drop in complex scenes with sparse or non-rigid deformations.

### B. Deep Learning-based Correspondence Pruning

Following the pioneering work of LFGC [12], learning-based methods have dominated this field. Early approaches,

such as NM-Net [15] and OANet [21], employ CNNs or Graph Neural Networks (GNNs) to capture local topological structures. Specifically, CLNet [16] and NCMNet [17] propose progressive pruning strategies by constructing dynamic graphs to mine local consensus. MS<sup>2</sup>DG-Net [28] further improves performance by integrating sparse semantic information into dynamic graph learning. Recently, Transformer-based methods have achieved remarkable success by modeling global contexts. VSFormer [13] and TransMatch [14] utilize self-attention mechanisms to capture long-range dependencies between correspondences. Similarly, CLG-Net [29] and MGCA-Net [30] introduce lightweight attention modules to balance local and global perceptions. However, these methods still face challenges: GNN-based approaches often suffer from feature over-smoothing during propagation, while Transformer-based methods are limited by quadratic computational complexity. These limitations highlight the need for a more efficient architecture.

### C. State Space Models

State Space Models (SSMs) have garnered significant interest in recent years for their potential to model long sequences with linear computational complexity. Notably, the Structured State Space sequence model (S4) [19] effectively captures long-range dependencies, addressing the efficiency bottlenecks of traditional attention mechanisms. Building on this foundation, Mamba [18] introduces a data-dependent selective scan mechanism to overcome the limitations of time-invariant models, achieving remarkable success in natural language processing. Inspired by these advancements, researchers have extended Mamba to the computer vision domain. Vision Mamba (Vim) [31] and VMamba [32] employ bidirectional or cross-scanning strategies to model non-causal visual data, achieving performance comparable to Vision Transformers (ViT) [33]. Furthermore, recent works like PointMamba [34] have successfully applied SSMs to point cloud analysis, significantly reducing memory usage while maintaining performance. In the specific context of correspondence pruning, MatchMamba [20] are the pioneering works. They treat sparse correspondences as a sequence and leverage the Mamba block to efficiently capture global context. However, these methods predominantly operate in the spatial domain, overlooking the spectral distinction between inliers and outliers.

### D. Frequency Domain and Spectral Methods

Frequency domain analysis has gained increasing attention in computer vision for its inherent ability to decouple valid signals from noise and capture global context with linear complexity. In the field of multi-modal image fusion, SFMFusion [35] integrates frequency domain analysis with Mamba to capture complementary information and enhance global perception. Similarly, in dense prediction tasks, FM-Net [36] demonstrates the effectiveness of frequency-assisted attention in handling ambiguous features by suppressing high-frequency noise. GGSLC [37] leverages spectral graph theory to introduce a grid-guided sparse Laplacian consensus, enforcing smooth geometric constraints for robust matching. These

advancements motivate us to further explore the potential of integrating frequency domain analysis with State Space Models to achieve robust correspondence pruning.

## III. PROPOSED METHOD

This section starts with the problem formulation of correspondence pruning and outlines the overall pipeline of our proposed SFMambaNet. Subsequently, we elaborate on the two core components designed for feature enhancement: the Local Spectral-Geometric Attention (LSGA) block in Section III-C and the Spectral-Integrated Global Mamba (SIGM) block in Section III-D. Following the architectural details, we discuss the training objective function. The section concludes with the specific implementation settings.

### A. Problem Formulation

Given a pair of source and target images, we first employ standard feature detectors, such as SIFT [7] or SuperPoint [8], to extract keypoints and descriptors. By applying a nearest-neighbor search strategy to the extracted descriptors, we construct an initial correspondence set  $C$  of putative matches between the two images. The objective of this work is to identify correct correspondences in  $C$  and remove false matches. The set  $C$  is formulated as:

$$C = \{c_1, c_2, \dots, c_N\} \in \mathbb{R}^{N \times 4}, \quad (1)$$

where  $N$  denotes the number of the putative correspondences. Each element  $c_i = (u_i, v_i, u'_i, v'_i)$  represents a correspondence connecting the normalized keypoint coordinates  $(u_i, v_i)$  in the first image and  $(u'_i, v'_i)$  in the second image. In practice, this initial set  $C$  is inevitably contaminated by a significant proportion of outliers due to complex scene variations, which poses a severe challenge to robust geometric estimation.

The proposed SFMambaNet architecture, illustrated in Fig. 2, reformulates correspondence pruning as a binary classification task to distinguish inliers from outliers. To achieve this goal, we adopt an iterative pruning strategy as the main framework, since it effectively reduces the adverse influence of numerous outliers. Specifically, SFMambaNet first processes the input set  $C$  with two sequential pruning blocks. Each pruning block consists of two components, namely the Local Spectral-Geometric Feature Extractor (LSGFE) and the Spectral-Global Context Aggregator (SGCA). We then estimate a parametric model in the Verification Block. Finally, we use the estimated model to perform full-size verification on  $C$ , which helps prevent valid inliers from being mistakenly removed during the pruning process.

The initial correspondence set  $C$  is first mapped into a high-dimensional feature space. Then, fine-grained local spectral-geometric features are extracted by the LSGFE, while robust global frequency-aware context is aggregated by the SGCA. The integration of these two blocks facilitates the selection of more reliable correspondences. The network predicts a confidence weight set  $\mathcal{W}_2 = \{w_1, w_2, \dots, w_N\}$ , where each scalar  $w_i \in [0, 1)$  quantifies the likelihood of the  $i$ -th correspondence being an inlier. These weights drive the differentiable weighted eight-point algorithm to estimate the optimal essential matrix

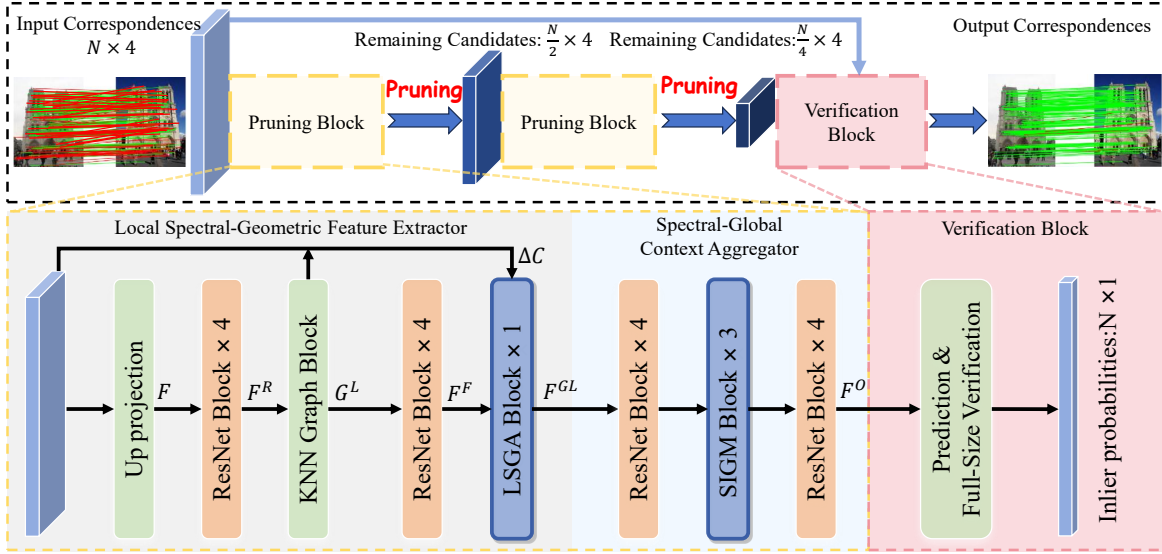


Fig. 2. The architecture of SFMambaNet. It takes  $N \times 4$  initial correspondences as inputs and outputs  $N \times 1$  inlier probabilities by an iterative pruning strategy, which distills more reliable candidates to estimate the parametric model. The Pruning block comprises a Local Spectral-Geometric Feature Extractor (LSGFE) and a Spectral-Global Context Aggregator (SGCA). The Verification block comprises prediction and full-size validation operations. Here, LSGA stands for Local Spectral-Geometric Attention block, and SIGM stands for Spectral-Integrated Global Mamba block.

$\hat{\mathbf{E}}$ . A subsequent full-size verification on the raw input set  $C$  maximizes recall by assessing symmetric epipolar errors against the estimated pose  $\hat{\mathbf{E}}$ . Adhering to the protocols established by CLNet [16] and MS<sup>2</sup>DGNet [28], we classify matches with a Sampson distance below the predefined threshold as final inliers. This verification step effectively recovers true positives that might have been aggressively pruned in earlier stages. The entire inference pipeline is formulated as:

$$\begin{aligned} (\mathcal{W}_1, C_1) &= f_{\theta_1}(C), & (\mathcal{W}_2, C_2) &= f_{\theta_2}(\mathcal{W}_1, C_1), \\ \hat{\mathbf{E}} &= g(\mathcal{W}_2, C_2), & \mathcal{D} &= h(\hat{\mathbf{E}}, C), \end{aligned} \quad (2)$$

where  $f_{\theta_1}(\cdot)$  and  $f_{\theta_2}(\cdot, \cdot)$  denote the two cascaded stages of SFMambaNet parameterized by  $\theta_1$  and  $\theta_2$ . The terms  $(\mathcal{W}_k, C_k)$  represent the output weights and the preserved subset at the  $k$ -th network output, respectively. The function  $g(\cdot, \cdot)$  signifies the weighted eight-point algorithm, and  $h(\cdot, \cdot)$  computes the set of epipolar distances  $\mathcal{D}$  for the final decision.

### B. Local Graph Construction (LGC) Block

To initiate the feature learning process, we project the raw correspondence set  $C$  into a high-dimensional manifold using a Multi-Layer Perceptron (MLP), yielding the preliminary embedding  $F = \{f_i\}_{i=1}^N \in \mathbb{R}^{D \times N \times 1}$ . Following the architectural design in [16],  $F$  is further processed by a sequence of ResNet blocks to acquire the refined deep feature representation  $F^R = \{f_i^R\}_{i=1}^N \in \mathbb{R}^{D \times N \times 1}$ . We construct an explicit local graph  $G^L = \{g_i^L\}_{i=1}^N$  to capture the topological structure centered at each correspondence. For the  $i$ -th node, its local subgraph is mathematically formulated as:

$$g_i^L = (\mathcal{V}_i^L, \mathcal{E}_i^L), \quad 1 \leq i \leq N, \quad (3)$$

where  $\mathcal{V}_i^L = \{f_j^R \mid 1 \leq j \leq k\}$  represents the set of  $k$ -nearest neighbors for the query node  $f_i^R$ . These neighbors

are dynamically retrieved by ranking the sparse semantic distance [28] between  $f_i^R$  and all other candidates  $\{f_j^R\}_{j \neq i}$ . Correspondingly,  $\mathcal{E}_i^L = \{e_{ij}^L \mid 1 \leq j \leq k\}$  denotes the set of edge features connecting the center node to its neighborhood. To explicitly encode both position-aware and differential information, the specific edge feature  $e_{ij}^L$  is defined as:

$$e_{ij}^L = [f_i^R, \Delta f_{ij}^R], \quad 1 \leq j \leq k, \quad (4)$$

where  $\Delta f_{ij}^R = f_i^R - f_{ij}^R$  signifies the local residual vector, and  $[\cdot, \cdot]$  denotes the channel-wise concatenation operation.

After constructing the explicit local graph  $G^L$ , we apply feature fusion on  $G^L$  using an MLP combined with max pooling, resulting in the fused feature set  $F^F \in \mathbb{R}^{D \times N \times 1}$  for the explicit local graph. The above operations can be represented as follows:

$$F^F = \text{MaxPooling}(\text{MLPs}(G^L)). \quad (5)$$

Although the constructed explicit local graph  $G^L$  provides basic neighborhood topology, EdgeConv-style aggregation applies an MLP and then max pooling, the update is dominated by large feature activations rather than discriminative structure. Small but informative high-frequency spatial perturbations, which often separate outliers from inliers, are consequently suppressed, making local verification fragile once the two classes overlap in the feature space. We therefore introduce the Spectral-Geometric Encoding operation, which injects high-frequency spatial priors into the local feature interaction to recover the missing geometric consistency.

### C. Local Spectral-Geometric Attention (LSGA) Block

As is known, existing correspondence pruning methods largely rely on feature similarity for neighborhood aggregation. However, this paradigm often struggles to capture fine-grained geometric structures, especially when outliers exhibit

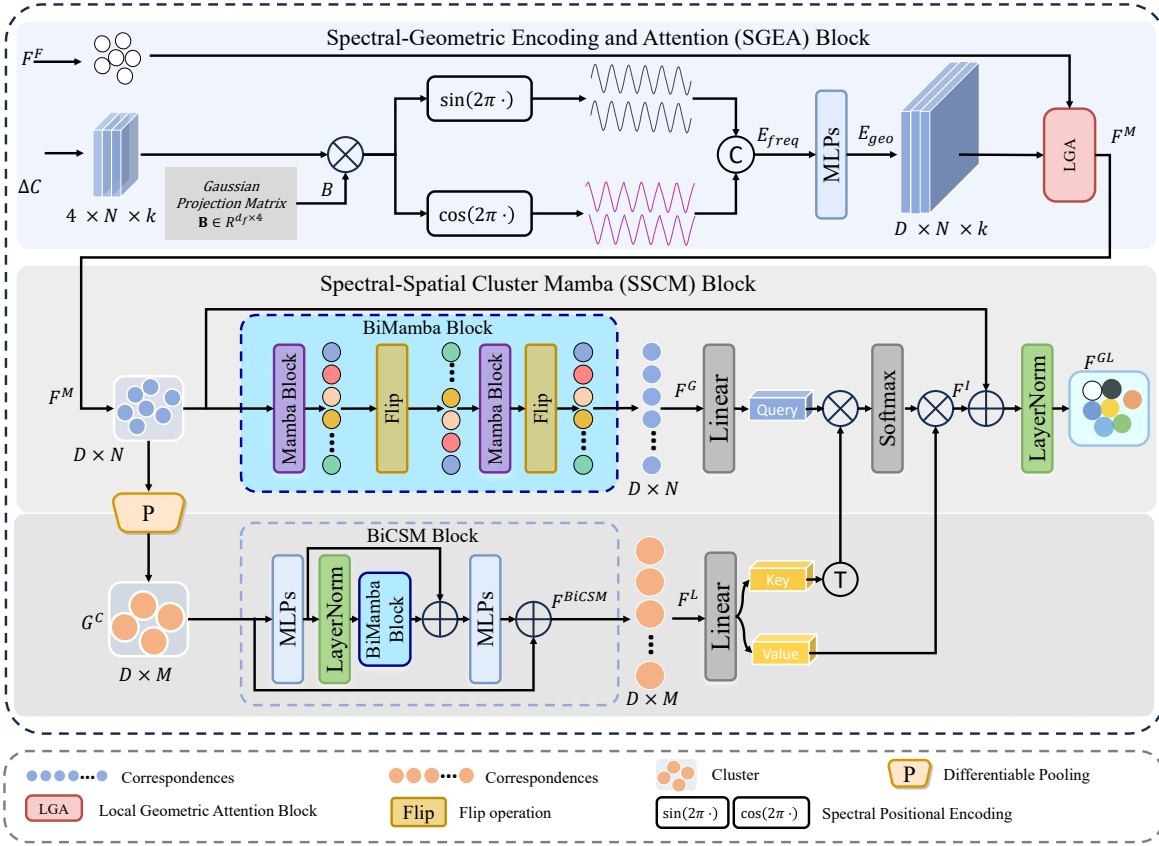


Fig. 3. Illustration of the LSGA block. The proposed LSGA block mainly consists of a Spectral-Geometric Encoding and Attention (SGEA) Block and a Spectral-Spatial Cluster Mamba (SSCM) Block. The SSCM Block features a dual-branch structure comprising a BiMamba branch for global point context and a Bidirectional Cluster Spatial Mamba (BiCSM) branch for regional consensus. The BiCSM block itself includes two MLP blocks, a LayerNorm block, and a Bidirectional Mamba block to refine spatial relationships within clusters.  $F^F$  is the explicit local graph feature set. After being processed by the geometry-infused attention mechanism,  $F^M$  captures subtle geometric structures.  $G^C$  is the cluster feature set after coarsening by DiffPooling and is processed by BiCSM. Finally, to fuse microscopic and macroscopic contexts, the cluster-aware features  $F^L$  interact with the global feature  $F^G$  through a Multi-Scale Interaction mechanism, yielding the final fine-grained feature set  $F^{GL}$ .

high local ambiguity. In this section, we propose the Local Spectral-Geometric Attention (LSGA) block. Unlike GNNs that treat neighbors equally, LSGA integrates frequency domain analysis into local graph learning to enhance geometric discriminability. As shown in Fig. 3, the LSGA block comprises two key components: Spectral-Geometric Encoding and Attention (SGEA) Block, and Spectral-Spatial Cluster Mamba (SSCM) Block.

1) *Spectral-Geometric Encoding and Attention (SGEA) Block*: This block implements the Spectral-Geometric Encoding operation and couples it with local attention. Given  $C \in \mathbb{R}^{N \times 4}$ , for each correspondence  $c_i \in C$ , we retrieve the coordinates of its  $k$ -nearest neighbors based on the indices in  $\mathcal{V}_i^L$  (from Eq. (3)) to form the neighbor coordinate tensor  $C_{\mathcal{N}} \in \mathbb{R}^{4 \times N \times k}$ . We then compute the relative coordinate matrix  $\Delta C$  by subtracting the central coordinate  $c_i$  from its neighbors:  $\Delta C = C_{\mathcal{N}} - c_i^{broadcast}$ , where  $\Delta C \in \mathbb{R}^{4 \times N \times k}$ . Instead of directly using these low-dimensional Euclidean coordinates as geometric cues, we map them into a high-dimensional frequency spectrum via Fourier features [38] to perceive subtle geometric fluctuations. Specifically, given a fixed random Gaussian projection matrix  $\mathbf{B} \in \mathbb{R}^{d_f \times 4}$ , we

generate the spectral position encoding  $E_{freq}$  as:

$$E_{freq} = \text{Concat}(\sin(2\pi \mathbf{B} \Delta C), \cos(2\pi \mathbf{B} \Delta C)), \quad (6)$$

where  $E_{freq} \in \mathbb{R}^{2d_f \times N \times k}$ , and  $2d_f$  denotes the projection dimension. This frequency spectrum provides discriminative high-frequency priors, enabling the network to distinguish geometrically consistent inliers from random outliers.

To incorporate frequency-aware geometric information into local neighborhood interaction, we introduce  $E_{freq}$  into the attention computation. First, based on the indices in the local graph  $G^L$ , we gather the node features from given  $F^F$  (from Eq. (5)) corresponding to the  $k$ -nearest neighbors to form a neighbor feature tensor  $F_{\mathcal{N}}^F \in \mathbb{R}^{D \times N \times k}$ . Similarly, the fused feature set  $F^F$  is reshaped to  $\mathbb{R}^{D \times N \times 1}$  to serve as the query source. The frequency encoding  $E_{freq}$  is mapped to the feature space to obtain the geometric embedding  $E_{geo} = \text{MLP}(E_{freq}) \in \mathbb{R}^{D \times N \times k}$ .

We then compute the local geometric attention (LGA), as shown in Fig. 4. The Query ( $Q$ ), Key ( $K$ ), and Value ( $V$ ) tensors are projected as:

$$\begin{aligned} Q &= W_Q F^F, & \in \mathbb{R}^{D \times N \times 1} \\ K &= W_K (F_{\mathcal{N}}^F + E_{geo}), & \in \mathbb{R}^{D \times N \times k} \\ V &= W_V (F_{\mathcal{N}}^F + E_{geo}), & \in \mathbb{R}^{D \times N \times k}, \end{aligned} \quad (7)$$

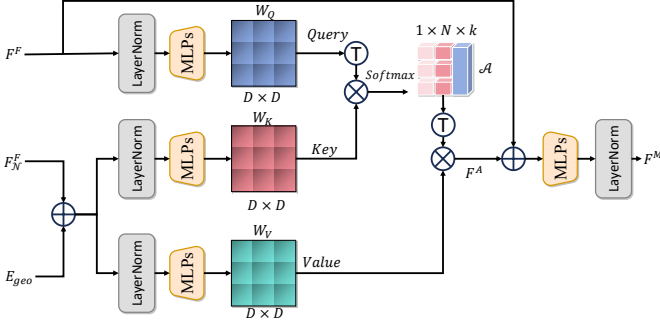


Fig. 4. Details of Local Geometric Attention (LGA) Block. The central feature  $F^F$  ( $D \times N \times 1$ ) acts as the Query, while the neighbor features  $F_N^F$  ( $D \times N \times k$ ) are fused with the spectral-geometric embedding  $E_{geo}$  to formulate the Key and Value. The attention map is generated by projecting the Query onto the Key along the channel dimension. Finally, the aggregated features are computed by weighting the Value with the attention map, producing the output  $F^M$  with consistent dimensions.

where  $W_Q, W_K, W_V \in \mathbb{R}^{D \times D}$  are learnable projection matrices. For two tensors  $X \in \mathbb{R}^{a \times N \times b}$  and  $Y \in \mathbb{R}^{b \times N \times c}$ , we define the  $N$ -wise batched matrix product  $\text{BMM}_N(X, Y) \in \mathbb{R}^{a \times N \times c}$  as  $[\text{BMM}_N(X, Y)]_{:,i,:} = X_{:,i,:} Y_{:,i,:}$  for  $i = 1, \dots, N$ . The geometry-aware local aggregation is then performed. We compute the attention map  $\mathcal{A}$  via a dot product over the channel dimension  $D$ :

$$\mathcal{A} = \text{Softmax}\left(\frac{\text{BMM}_N(Q^\top, K)}{\sqrt{D}}\right) \in \mathbb{R}^{1 \times N \times k}, \quad (8)$$

where  $Q^\top \in \mathbb{R}^{1 \times N \times D}$  denotes the tensor obtained by swapping the first and third dimensions of  $Q$ . The Softmax is applied along the neighbor dimension  $k$ , so each center distributes its attention only over its local neighbors. Finally, the aggregated feature  $F^A$  is obtained by applying the  $N$ -wise batched product between the Value  $V$  and the attention map  $\mathcal{A}$ :

$$F^A = \text{BMM}_N(V, \mathcal{A}^\top) \in \mathbb{R}^{D \times N \times 1}, \quad (9)$$

where  $\mathcal{A}^\top \in \mathbb{R}^{k \times N \times 1}$  is obtained by swapping the first and third dimensions of  $\mathcal{A}$ . Because each center only attends to its  $k$  nearest neighbors, the attention cost scales as  $\mathcal{O}(NkD)$  rather than  $\mathcal{O}(N^2D)$  required by full pairwise attention. The resulting  $F^A$  aggregates the local context, which is weighted by both feature similarity and spectral-geometric consistency.

Finally, we integrate original feature information and geometry-infused interaction by a residual fusion:

$$F^M = \text{LayerNorm}(\text{MLPs}(F^F + F^A)). \quad (10)$$

Here,  $F^M \in \mathbb{R}^{D \times N \times 1}$  denotes the LSGA-refined local feature set, which will be further processed by the subsequent SSCM block.

2) *Spectral-Spatial Cluster Mamba (SSCM) Block*: Following the injection of high-frequency geometric priors in the previous steps, the feature representation  $F^M$  effectively encodes point-wise spectral-geometric consistency. However, relying solely on fine-grained point features is insufficient to capture region-level structural consensus. To address this,

we propose the SSCM component, which constructs a dual-branch architecture with Bidirectional Mamba (BiMamba) and Bidirectional Cluster Spatial Mamba (BiCSM), and Multi-Scale Spectral Interaction.

First, to establish regional consensus and a stable scan axis, we employ differentiable pooling (DiffPool) [39] to group the unordered features  $F^M$  into a set of canonical-order clusters  $G^C \in \mathbb{R}^{D \times M \times 1}$ , where  $M \ll N$ . The assignment scores produced by DiffPool are also used to derive a cluster-induced permutation  $\Pi$ , which arranges point-level correspondences according to their dominant cluster indices. Simultaneously, we process the reordered fine-grained features in a parallel branch using a standard bidirectional Mamba to capture global dependencies, and then restore the original correspondence order for point-wise prediction, denoted as  $F^G \in \mathbb{R}^{D \times N \times 1}$ . This dual-scale preparation is formulated as:

$$\begin{aligned} G^C, S &= \text{DiffPool}(F^M), \\ \Pi &= \text{Order}(S), \\ F^G &= \Pi^{-1}(\text{BiMamba}(\Pi(F^M))), \end{aligned} \quad (11)$$

where  $S \in \mathbb{R}^{N \times M}$  denotes the soft assignment matrix,  $\text{Order}(\cdot)$  groups correspondences by the fixed cluster-slot indices indicated by  $S$ ,  $\Pi(\cdot)$  applies the resulting permutation, and  $\Pi^{-1}(\cdot)$  restores the original correspondence order. In this way, the Mamba scan is performed on a geometry-aware regional sequence rather than on an arbitrary input order. The canonical ordering of clusters therefore provides a natural structural basis for subsequent spatial-frequency context modeling.

Then,  $G^C$  is fed into the Bidirectional Cluster Spatial Mamba (BiCSM) block for spatial information aggregation, resulting in aggregated cluster graph features  $F^{BiCSM} \in \mathbb{R}^{D \times M \times 1}$ . As shown in Fig. 3, the BiCSM consists of two MLP blocks, a LayerNorm block, a Bidirectional Mamba block, and a skip connection. Unlike the original Mamba block, which performs feature selection and filtering along the channel dimension, the BiCSM block first transposes the spatial and channel dimensions of the correspondences. It then applies a weight-sharing perceptron along the spatial dimension to establish spatial relationships between correspondences. Furthermore, different from OANet, which aggregates spatial features without distinction, the BiCSM block leverages the Mamba selection mechanism [40], [41] to dynamically select features with higher spatial consistency based on their importance, thereby producing more robust local feature representations. The operation is formulated as:

$$F^{BiCSM} = \text{BiCSM}(G^C), \quad (12)$$

where  $\text{BiCSM}(\cdot)$  represents the Cluster Spatial Mamba operation.

Finally, to facilitate information flow between the microscopic global context and macroscopic regional structures, we introduce a Multi-Scale Interaction mechanism. We first denote the cluster-aware features as  $F^L$ :

$$F^L = F^{BiCSM}, \quad (13)$$

where  $F^L \in \mathbb{R}^{D \times M \times 1}$ . For computational convenience, we then squeeze the global point features into  $F^G \in \mathbb{R}^{D \times N}$  (from

Eq. (11)) as Queries, and the cluster-aware features into  $F^L \in \mathbb{R}^{D \times M}$  as Keys and Values to compute the interaction feature  $F^I$ :

$$F^I = F^L (\text{Softmax} \left( \frac{(F^L)^\top F^G}{\sqrt{D}} \right)). \quad (14)$$

Through this interaction, the point-level global features are rectified by the stable regional consensus. The final output of the LSGA block,  $F^{GL}$ , is obtained by fusing the interaction result with the input residual:

$$F^{GL} = \text{LayerNorm}(F^M + F^I), \quad (15)$$

where  $F^{GL} \in \mathbb{R}^{D \times N \times 1}$  denotes the final set of local spectral-geometric feature vectors.

#### D. Spectral-Integrated Global Mamba (SIGM) Block

The two spectral modules operate on different domains and play complementary roles. LSGA performs spectral expansion on local relative coordinates, aiming to enrich fine-grained geometric cues before message passing. In contrast, SIGM performs spectral filtering on globally propagated features, aiming to stabilize long-range context aggregation. Therefore, SFMambaNet combines local geometric frequency modeling with global sequence-level spectral filtering, rather than relying on a single notion of frequency perception.

While the LSGA block effectively extracts local spectral-geometric features, determining the correctness of a correspondence requires a robust global consensus. Existing methods like MatchMamba [20] employ the Correspondence-Flipped Bidirectional Mamba (CFBM) to model global context. However, they treat the correspondence sequence solely in the spatial domain. During long-range state transitions, high-frequency noise derived from outliers inevitably accumulates in the hidden states, diluting the geometric consistency of inliers. To address this ‘‘noise accumulation’’ issue, we propose the Spectral-Integrated Global Mamba (SIGM) block. By embedding the Frequency-domain gating operation into the sequential bidirectional scanning process, SIGM filters high-frequency noise at each stage of global feature propagation.

As illustrated in Fig. 5, SIGM performs a sequential process: a Forward Spectral Scan followed by a Backward Spectral Scan. We take the output of the LSGA block,  $F^{GL} \in \mathbb{R}^{D \times N \times 1}$ , as the input and reuse the cluster-induced permutation  $\Pi$  from Eq. (11) to obtain the ordered feature sequence  $F_{ord}^{GL} = \Pi(F^{GL})$ . After the spectral scans, the inverse permutation  $\Pi^{-1}$  restores the original correspondence order for the final point-wise output.

1) *Forward Scan with Frequency Gating*: The FFT-based filtering in Eq. (16) constitutes the Frequency-domain gating operation. First, we feed the cluster-ordered local feature map set  $F_{ord}^{GL}$ , obtained from LSGA, into a forward Mamba block. This step explicitly captures the causal dependency along the cluster-induced regional sequence, yielding the initial global feature  $F_{fwd} \in \mathbb{R}^{D \times N \times 1}$ . To suppress the accumulated noise before passing information to the backward stage, similar to the mechanism in Global Filter Networks [42], we project

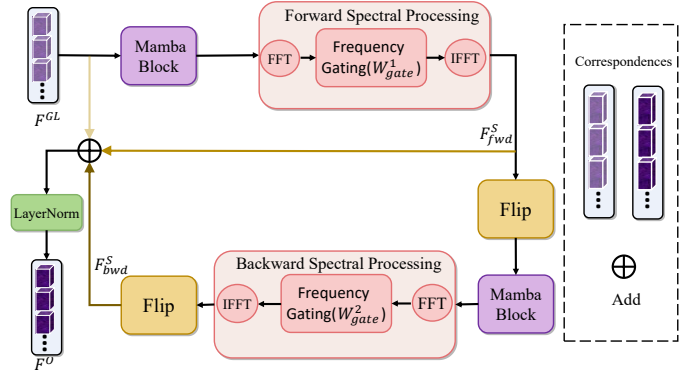


Fig. 5. Schematic diagram of the SIGM block. It consists of two Mamba blocks and two spectral frequency processing operations. By incorporating frequency gating and performing both forward and backward spectral scans, the Mamba blocks capture the global context more robustly, ultimately yielding the enhanced global graph feature set,  $F^O$ .

$F_{fwd}$  into the frequency domain via Fast Fourier Transform (FFT) and apply a learnable complex gating weight  $W_{gate}^1$  [42], [43]:

$$\begin{aligned} F_{fwd} &= \text{Mamba}(F_{ord}^{GL}), \\ \mathcal{F}_{fwd} &= \text{FFT}(F_{fwd}) \odot \text{Interp}(W_{gate}^1), \\ F_{fwd}^S &= \text{IFFT}(\mathcal{F}_{fwd}), \end{aligned} \quad (16)$$

where  $\odot$  denotes element-wise multiplication,  $\text{Interp}(\cdot)$  denotes the operation that handles dynamic sequence lengths, and  $F_{fwd}^S$  denotes the spectrally-refined forward context.

2) *Backward Scan with Forward Absorption*: Unlike independent bidirectional scanning, we adopt a sequential strategy to ensure the backward scan fully absorbs the forward context. Specifically, we flip the sequence of the purified forward feature  $F_{fwd}^S$  and feed it into a second Mamba block. This is followed by another spectral gating operation with weight  $W_{gate}^2$  to further refine the global consensus:

$$\begin{aligned} F_{bwd} &= \text{Mamba}(\text{Flip}(F_{fwd}^S)), \\ \mathcal{F}_{bwd} &= \text{FFT}(F_{bwd}) \odot \text{Interp}(W_{gate}^2), \\ F_{bwd}^S &= \text{IFFT}(\mathcal{F}_{bwd}). \end{aligned} \quad (17)$$

Through this process,  $F_{bwd}^S$  effectively integrates bidirectional information while maintaining spectral purity. The FFT-based gate acts as a Frequency-domain gating operation on the hidden state of the scan. Since the transform is performed along the sequence dimension for  $D$  channels, its per-forward-pass cost is  $\mathcal{O}(DN \log N)$ , which remains strictly subquadratic with respect to  $N$ .

Finally, to restore the original sequence order and preserve gradient flow, we flip the backward output again and fuse it with the forward context and the input residual:

$$F^O = \Pi^{-1} (\text{LayerNorm}(F_{ord}^{GL} + F_{fwd}^S + \text{Flip}(F_{bwd}^S))), \quad (18)$$

where  $\text{LayerNorm}(\cdot)$  and  $\text{Flip}(\cdot)$  represent the Layer Normalization and Flip operations, respectively, and  $F^O \in \mathbb{R}^{D \times N \times 1}$  denotes the final global feature set.

### E. Loss Function

To jointly optimize the network for both correspondence classification and camera pose estimation, we formulate the training objective as a hybrid loss function. This objective combines a binary classification loss with a geometric error term, such as OANet++ [21] and CLNet [16]:

$$\mathcal{L}_{total} = \mathcal{L}_{cls} + \gamma \mathcal{L}_{geo}(\hat{\mathbf{E}}, \mathbf{E}_{gt}), \quad (19)$$

where  $\mathcal{L}_{cls}$  denotes the binary cross-entropy loss applied to the classification predictions. The term  $\gamma$  serves as a balancing weight to harmonize the magnitude of the two losses.

The geometric loss  $\mathcal{L}_{geo}(\cdot)$  is derived using the Sampson distance to regress the predicted essential matrix toward the ground-truth one. Following precedents in [16], [21], it is formulated as:

$$\mathcal{L}_{geo}(\hat{\mathbf{E}}, \mathbf{E}_{gt}) = \frac{(\mathbf{p}'_i{}^\top \hat{\mathbf{E}} \mathbf{p}_i)^2}{\|\mathbf{E}_{gt} \mathbf{p}_i\|_{[1]}^2 + \|\mathbf{E}_{gt} \mathbf{p}_i\|_{[2]}^2 + \|\mathbf{E}_{gt}^\top \mathbf{p}'_i\|_{[1]}^2 + \|\mathbf{E}_{gt}^\top \mathbf{p}'_i\|_{[2]}^2}, \quad (20)$$

where  $\hat{\mathbf{E}}$  and  $\mathbf{E}_{gt}$  denote the predicted essential matrix and ground-truth essential matrix, respectively;  $\mathbf{p}_i$  and  $\mathbf{p}'_i$  are virtual correspondence coordinates generated by  $\mathbf{E}_{gt}$ ; and  $\|\cdot\|_{[1]}$  and  $\|\cdot\|_{[2]}$  represent the first and second elements of the vector.

### F. Implementation Details

Implemented in PyTorch, the framework processes inputs of  $N = 2000$  putative correspondences derived from standard descriptors such as SIFT [7] or SuperPoint [8]. Model hyperparameters include a channel dimension  $D$  of 128 and a Fourier projection dimension  $d_f$  in Eq. (6) fixed at 64. Structural parameters initiate the number of clusters  $m$  at 256 and neighbors  $k$  at 18, while state space configurations for the Mamba components are set to 8 for the LSGA block and 16 for the SIGM block. Optimization utilizes the Adam solver [44] with a batch size of 32 over 500k iterations. The scheduling strategy employs a linear warm-up from an initial learning rate of  $10^{-3}$  during the first 10k steps, followed by a decay factor of 0.4 applied every 20k steps. Adhering to the CLNet [16] protocol, a symmetric epipolar distance threshold of  $10^{-4}$  identifies correct matches. Dynamic adjustment of the loss weight  $\gamma$  in Eq. (19) harmonizes multi-task objectives by maintaining a value of 0 for the first 20k iterations to prioritize classification before settling at 0.5. Computing resources consist of a single NVIDIA RTX 3090 GPU running on Ubuntu 22.04.

## IV. EXPERIMENTS

To rigorously evaluate the performance and generalization capability of the proposed SFMambaNet, we conducted comprehensive experiments across the following distinct tasks: camera pose estimation, outlier removal, homography estimation. This section details the experimental setup, provides

a comparative analysis against state-of-the-art methods, and presents an ablation study to verify the efficacy of the proposed LSGA and SIGM modules, as well as the impact of hyperparameter configurations.

### A. Evaluation Protocol

1) *Datasets*: Our evaluations are performed on two standard benchmarks representing diverse environments, namely outdoor YFCC100M [45] and indoor SUN3D [46]. The YFCC100M dataset comprises a vast collection of internet tourist landmark images with varied illumination and geometry, whereas SUN3D consists of indoor sequences captured from RGB-D videos. Adhering to the widely adopted split protocol established by OANet [21], we utilize 68 sequences for training and 4 for testing on YFCC100M. Similarly, for SUN3D, the dataset is partitioned into 239 training sequences and 15 testing sequences. To ensure robust training, the training sequences are further stratified into 60% training, 20% validation, and 20% testing subsets, respectively. It is worth noting that the designated test sequences remain unseen during the training phase to assess generalization.

2) *Evaluation Metrics*: For camera pose estimation, we quantify accuracy by calculating the angular error between the ground truth and the rotation and translation vectors recovered from the essential matrix. Following established protocols [21], we report the mean Average Precision (mAP) at error thresholds of  $5^\circ$  and  $20^\circ$ . For outlier rejection, we assess the classification quality using Precision, Recall, and F-score. Specifically, F-score serves as a comprehensive metric to balance precision and recall, evaluating the overall effectiveness of the model in distinguishing inliers from mismatches.

### B. Camera Pose Estimation

We evaluate the precision of SFMambaNet in recovering the relative camera geometry between image pairs, a prerequisite for downstream applications like 3D reconstruction [47]. The evaluation utilizes standard SIFT and SuperPoint descriptors to generate initial inputs. We compare SFMambaNet with various state-of-the-art methods, including the traditional RANSAC [9] algorithm and learning-based approaches such as PointNet++ [48], LFGC [12], SuperGlue [49], OANet++ [21], ACNe [50], T-Net [51], CLNet [16], MS<sup>2</sup>DGNet [28], U-Match [52], PGFNet [53], NCMNet [17], MGNet [54], MS-GSA [55], BCLNet [56], and MatchMamba [20].

**Results on SIFT features.** Quantitative comparisons on indoor SUN3D and outdoor YFCC100M are summarized in Table I. SFMambaNet establishes a new state-of-the-art across all metrics. Specifically, under the challenging unknown split on outdoor YFCC100M, our method achieves a remarkable margin of 6.23% in mAP $5^\circ$  over the second best method MatchMamba [20], while extending this lead to 2.19% under the known split on outdoor YFCC100M. For indoor SUN3D, SFMambaNet yields consistent gains of 3.02% and 1.00% in known and unknown splits, respectively. These results indicate that SFMambaNet effectively captures fine-grained local geometric context via spectral-geometric encoding. By explicitly suppressing high-frequency noise through the integrated

TABLE I

PERFORMANCE COMPARISON OF CAMERA POSE ESTIMATION ON OUTDOOR YFCC100M AND INDOOR SUN3D, EVALUATED IN BOTH KNOWN AND UNKNOWN SCENES USING THE SIFT DESCRIPTOR. MAP5° (%) IS REPORTED WITHOUT THE USE OF RANSAC, WITH THE BEST PERFORMANCE HIGHLIGHTED IN BOLD AND THE SECOND-BEST RESULT UNDERLINED.

Matcher	YFCC100M (%)		SUN3D (%)	
	Known	Unknown	Known	Unknown
RANSAC [9]	5.81	16.88	4.73	3.26
PointNet++ [48]	10.49	16.48	10.58	8.10
LFGC [12]	13.81	23.95	13.78	11.40
OANet++ [21]	32.57	38.95	20.86	16.18
ACNe [50]	29.17	33.06	18.86	14.12
SuperGlue [49]	35.00	48.12	22.50	17.11
T-Net [51]	44.49	52.28	24.96	19.71
CLNet [16]	39.00	54.05	20.62	16.95
MS <sup>2</sup> DGNet [28]	38.36	49.13	22.20	17.84
PGFNet [53]	44.2	53.70	23.66	19.32
U-Match [52]	46.78	60.22	24.99	18.13
NCMNet [17]	52.39	63.52	<u>25.72</u>	20.82
MGNNet [54]	49.67	63.63	25.66	20.70
MSGSA [55]	54.94	64.95	25.28	20.41
BCLNet [56]	52.62	66.08	24.59	19.96
MatchMamba [20]	<u>60.09</u>	<u>67.60</u>	25.70	<u>20.97</u>
SFMambaNet(Ours)	<b>62.28</b>	<b>73.83</b>	<b>28.74</b>	<b>21.97</b>

frequency gating mechanism, it mitigates the accumulation of inconsistent features inherent to the application of standard Mamba in correspondence pruning and models global context with appropriate complexity, thereby significantly enhancing performance in camera pose estimation tasks, as analyzed in Section III-D.

**Results on SuperPoint features.** Extended evaluations with SuperPoint descriptors on outdoor YFCC100M, as reported in Table II, further confirm the generalization capability of our model. SFMambaNet maintains its superiority, outperforming the second best approach by 6.08% and 6.63% under the known and unknown splits on outdoor YFCC100M, respectively. This consistency across different descriptors underscores the adaptability and robustness of the spectral-frequency architecture in handling varying feature distributions.

### C. Outlier Removal

Outlier removal aims to remove mismatches to establish reliable correspondences, a critical capability for robust visual perception. We compare SFMambaNet with various state-of-the-art methods, including the traditional RANSAC [9] algorithm and learning-based approaches such as PointNet++ [48], LFGC [12], OANet++ [21], ACNe [50], T-Net [51], CLNet [16], MS<sup>2</sup>DGNet [28], PGFNet [53], U-Match [52], NCMNet [17], MSGSA [55], GCTNet [57], BCLNet [56], and MatchMamba [20].

**Quantitative Results.** Table III details the Precision, Recall, and F-score on outdoor YFCC100M and indoor SUN3D. SFMambaNet demonstrates exceptional robust estimation capabilities, achieving the highest Precision and F-score on outdoor YFCC100M and indoor SUN3D across known and unknown splits. Specifically, compared to the strong competitor MatchMamba [20], SFMambaNet reaches higher Precision and F-score than competing baselines on known and

TABLE II

PERFORMANCE COMPARISON OF CAMERA POSE ESTIMATION ON OUTDOOR YFCC100M IN BOTH KNOWN AND UNKNOWN SCENES USING THE SUPERPOINT DESCRIPTOR. MAP5°/MAP20° (%) SCORES ARE REPORTED, WITH THE BEST PERFORMANCE HIGHLIGHTED IN BOLD AND THE SECOND-BEST RESULT UNDERLINED.

Matcher	Known		Unknown	
	5° (%)	20° (%)	5° (%)	20° (%)
RANSAC [9]	12.85	31.22	17.47	38.83
LFGC [12]	12.18	34.75	24.25	52.70
OANet++ [21]	29.52	53.76	35.27	66.81
ACNe [50]	26.72	49.29	32.98	62.68
T-Net [51]	34.97	57.50	40.65	70.36
CLNet [16]	27.56	50.82	39.19	67.37
MS <sup>2</sup> DGNet [28]	31.15	55.16	39.19	70.36
U-Match [52]	35.01	56.80	44.29	70.90
NCMNet [17]	38.92	61.28	48.20	74.71
GCTNet [57]	37.86	60.55	47.17	74.76
MGNNet [54]	39.04	60.99	48.10	75.82
BCLNet [56]	40.56	62.71	48.07	75.84
MatchMamba [20]	<u>44.12</u>	<u>64.43</u>	<u>52.19</u>	<u>77.71</u>
SFMambaNet(Ours)	<b>50.20</b>	<b>70.10</b>	<b>58.82</b>	<b>81.04</b>

unknown splits for both datasets. However, it is noteworthy that SFMambaNet’s recall is slightly lower than some benchmark methods like U-Match [52]. This behavior stems from our rigorous pruning strategy, where SFMambaNet prioritizes high-confidence correspondences to ensure an accurate initial essential matrix estimation, which subsequently guides the full-size verification. While this aggressive filtering may discard ambiguous inliers, it significantly purifies the final correspondence set. The superior F-score confirms that this design choice effectively balances quantity and quality, leading to better overall matching performance.

**Qualitative Visualization.** To intuitively demonstrate the superiority of our method, Fig. 6 visualizes the matching results in challenging scenes characterized by extreme viewpoint changes and repetitive textures. Compared with baselines such as BCLNet [56], and MatchMamba [20], SFMambaNet successfully preserves a denser set of correct matches (green lines) while effectively suppressing outliers (red lines), verifying its robustness in complex geometric transformations.

### D. Homography Estimation

We investigate the robustness of SFMambaNet to planar geometric changes by conducting homography estimation. In this setting, the homography is inferred from correspondences to describe the projective relation between two views of the same plane. We conduct evaluations on the HPatches dataset [58], comprising 116 sequences characterized by significant illumination variations and viewpoint changes. Initial correspondences are generated by extracting top-4000 keypoints using SIFT, followed by a standard nearest neighbor search. Adhering to established protocols [8], we quantify performance using the percentage of correctly estimated homographies whose average corner reprojection error falls below thresholds of 3, 5, and 10 pixels.

We compare SFMambaNet with a series of representative methods trained on outdoor YFCC100M using SIFT descriptors, including PointCN [12], OANet++ [21], CLNet [16],

TABLE III  
QUANTITATIVE EVALUATION OF OUTLIER REMOVAL PERFORMANCE ON OUTDOOR YFCC100M AND INDOOR SUN3D, REPORTING PRECISION, RECALL, AND F-SCORE.

Methods	YFCC100M			SUN3D		
	P (%)	R (%)	F (%)	P (%)	R (%)	F (%)
RANSAC [9]	41.83	57.08	48.28	44.11	46.42	45.24
PointNet++ [48]	48.42	61.16	54.05	45.64	83.43	59.00
LFGC [12]	53.12	85.51	65.53	47.24	83.45	60.32
OANet++ [21]	55.65	85.80	67.51	46.54	83.43	59.74
ACNe [50]	54.56	86.92	67.04	46.44	84.23	59.87
T-Net [51]	57.48	88.38	69.66	46.94	84.53	60.36
CLNet [16]	74.89	76.79	75.83	59.97	84.55	64.73
MS <sup>2</sup> DGNet [28]	59.11	88.4	70.85	46.95	84.55	60.37
PGFNet [53]	57.54	88.77	69.82	47.05	85.02	60.58
U-Match [52]	60.30	<b>90.63</b>	72.42	47.59	<b>85.59</b>	61.17
NCMNet [17]	77.26	78.57	77.91	61.00	68.93	64.78
MSGSA [55]	60.43	89.01	71.98	47.99	84.32	61.22
GCTNet [57]	77.00	79.02	78.00	61.12	69.34	64.31
BCLNet [56]	78.49	82.56	80.10	77.39	79.77	78.31
MatchMamba [20]	80.53	84.27	82.36	78.27	80.04	79.15
SFMambaNet(Ours)	<b>82.49</b>	85.37	<b>83.16</b>	<b>80.05</b>	83.49	<b>81.51</b>

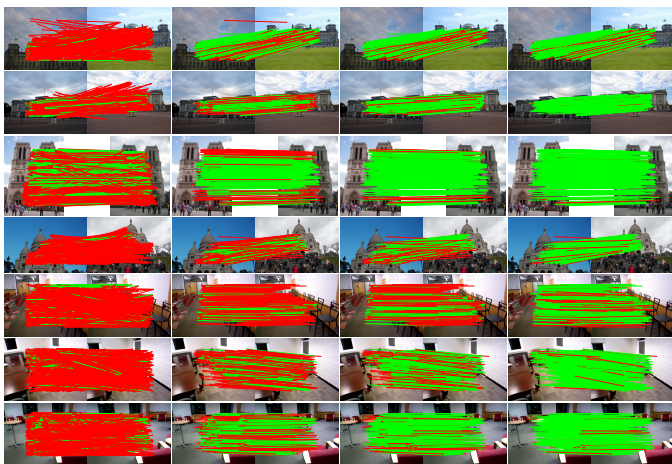


Fig. 6. Partial visualization results of outlier removal. From left to right are the results of Input, BCLNet, MatchMamba and SFMambaNet, respectively. From top to bottom the first four examples are taken from the unknown split on outdoor YFCC100M, while the others are derived from the unknown split on indoor SUN3D. These image pairs present substantial challenges, such as perspective changes, occlusions, repeating patterns, and textureless regions. Green lines represent inliers, and red lines represent outliers.

MS<sup>2</sup>DGNet [28], NCMNet [17], BCLNet [56], and the recent MatchMamba [20]. As detailed in Table IV, our proposed SFMambaNet outperforms all compared methods under all error thresholds. As shown in Fig. 7, which more intuitively demonstrates the superiority of our method, this result underscores the effectiveness of our spectral-frequency design in filtering outliers and recovering precise geometric transformations, even when applied to unseen planar scenes.

### E. Ablation Study

We conduct component ablations and complementary analyses on outdoor YFCC100M to examine how the proposed spectral-frequency modeling contributes to camera pose estimation. We first evaluate the main components of SFMambaNet under the known and unknown splits using mAP5°

TABLE IV  
PERFORMANCE EVALUATION OF HOMOGRAPHY ESTIMATION ON THE HPATCHES DATASET.

Methods	HPatches(%)		
	ACC.3PX	ACC.5PX	ACC.10PX
PointCN [12]	67.93	82.59	92.76
OANet++ [21]	69.66	82.93	91.90
CLNet [16]	69.83	81.55	90.69
MS <sup>2</sup> DGNet [28]	65.00	78.97	88.45
NCMNet [17]	70.69	81.90	91.03
BCLNet [56]	70.92	82.87	91.57
MatchMamba [20]	71.55	84.66	92.23
SFMambaNet(Ours)	<b>73.00</b>	<b>85.47</b>	<b>92.81</b>

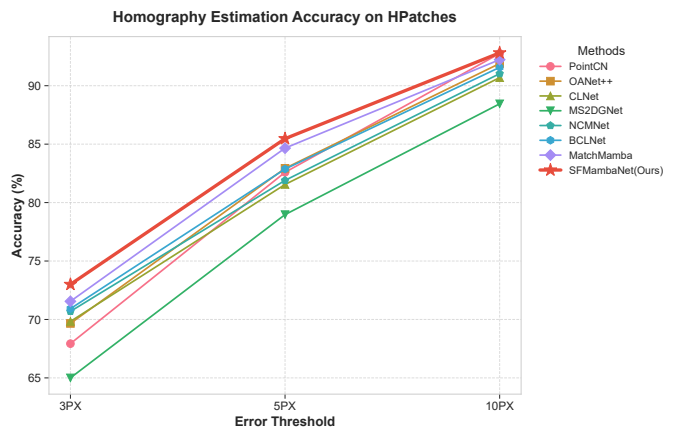


Fig. 7. Visualization of the performance evaluation curves for homography estimation on the HPatches dataset. The x-axis represents the error threshold in pixels (3PX, 5PX, and 10PX), and the y-axis indicates the corresponding estimation accuracy (%).

and mAP20°, and then decompose LSGA to verify the effect of its internal spectral-geometric encoding, bidirectional Mamba aggregation, hierarchical clustering, and multi-scale interaction. Beyond these ablations, we compare FLOPs, parameter size, training latency, and inference latency with representative correspondence pruning networks to assess the accuracy-efficiency trade-off. Finally, we analyze the scanning strategy in SIGM and provide a frequency-domain diagnostic to verify whether the proposed frequency gate suppresses unstable high-frequency components while preserving low-frequency geometric consensus.

**Proposed Main Components.** We initiate our analysis by scrutinizing the individual contributions of the LSGA and SIGM modules. Quantitative results presented in Table V illustrate that the progressive integration of these components into the baseline architecture yields consistent performance enhancements. Specifically, the complete SFMambaNet achieves a substantial 17.86% improvement in mAP5° over the baseline under the unknown split on outdoor YFCC100M. It is worth noting that the configuration utilizing only LSGA surpasses the variant utilizing only SIGM by 2.57% under the known split on outdoor YFCC100M. This superiority highlights the capability of LSGA to extract fine-grained local geometric details, effectively compensating for the limitations of GNNs in perceiving subtle structural variations. Further-

TABLE V  
ABLATION STUDY OF THE MAIN COMPONENTS OF SFMAMBA<sub>NET</sub> ON OUTDOOR YFCC100M, REPORTING MAP5° AND MAP20° RESULTS FOR KNOWN AND UNKNOWN SCENES WITHOUT RANSAC.

Components		Known		Unknown			
Baseline	Mamba	SIGM	LSGA	mAP5°	mAP20°	mAP5°	mAP20°
✓				40.37	61.11	55.97	75.21
✓	✓			50.21	69.57	63.18	81.75
✓		✓		52.21	73.59	66.60	83.89
✓			✓	54.78	74.98	64.88	83.48
✓	✓		✓	55.67	76.56	65.44	83.67
✓		✓	✓	<b>62.28</b>	<b>79.50</b>	<b>73.83</b>	<b>87.21</b>
✓	✓	✓	✓	60.91	78.06	72.18	85.76

more, a direct comparison between the second and third rows reveals that SIGM consistently outperforms the standard unidirectional Mamba, increasing mAP5° from 50.21%/63.18% to 52.21%/66.60% under the known/unknown splits. This finding confirms that SIGM leverages frequency features to aggregate correspondence information more robustly, thereby strengthening global context modeling. To ensure experimental fairness, we maintain an identical number of blocks when evaluating the unidirectional Mamba and SIGM, as both serve as global context aggregators. Notably, the last row, which activates the baseline, vanilla Mamba, SIGM, and LSGA simultaneously, does not further improve the results. Instead, its performance decreases by approximately 1–2% compared with the Baseline+SIGM+LSGA setting. This suggests that the additional vanilla Mamba module introduces redundant ungated state-space propagation, which can re-amplify high-frequency outlier responses and weaken the selective spectral filtering imposed by SIGM. It may also over-mix the local cues produced by LSGA, reducing feature discriminability. Therefore, we adopt Baseline+SIGM+LSGA as the final SFMambaNet configuration.

TABLE VI  
ABLATION STUDY ON THE PERFORMANCE GAINS OF KEY COMPONENTS IN LSGA ON THE UNKNOWN SPLIT OF OUTDOOR YFCC100M, REPORTING MAP5° AND MAP20° RESULTS WITHOUT RANSAC. **S<sub>GEA</sub>**: SPECTRAL-GEOMETRIC ENCODING AND ATTENTION. **B<sub>I</sub>MAMBA**: BIDIRECTIONAL MAMBA. **D<sub>P</sub>**: DIFFPOOL. **B<sub>I</sub>C<sub>S</sub>M**: BIDIRECTIONAL CLUSTER SPATIAL MAMBA. **M<sub>S</sub>I**: MULTI-SCALE INTERACTION.

Baseline	S <sub>GEA</sub>	B <sub>I</sub> Mamba	D <sub>P</sub>	B <sub>I</sub> C <sub>S</sub> M	M <sub>S</sub> I	mAP5°	mAP20°
✓						55.97	75.21
✓	✓					59.42	78.36
✓	✓	✓				61.08	80.12
✓	✓	✓	✓			62.33	81.29
✓	✓	✓	✓	✓		63.59	82.41
✓	✓	✓	✓	✓	✓	<b>64.88</b>	<b>83.48</b>

**Internal components of LSGA.** We further construct an internal ablation study to examine the contribution of each design in LSGA on the unknown split of outdoor YFCC100M. As reported in Table VI, the performance increases steadily as S<sub>GEA</sub>, B<sub>I</sub>Mamba, D<sub>P</sub>, B<sub>I</sub>C<sub>S</sub>M, and M<sub>S</sub>I are incrementally introduced into the baseline. S<sub>GEA</sub> provides the first major gain by injecting spectral-geometric cues into local attention, indicating that frequency-aware local encoding improves the discrimination of subtle geometric consistency. Adding Bi-

TABLE VII  
COMPUTATIONAL EFFICIENCY ANALYSIS OF SFMAMBA<sub>NET</sub> ON THE UNKNOWN SPLIT OF OUTDOOR YFCC100M WITH SIFT FEATURES, COMPARING MAP5° (%), PARAMETER SIZE (PARAMS, M), FLOATING-POINT OPERATIONS (FLOPS, G), AVERAGE RUNTIME PER EPOCH (ART, MS), AND AVERAGE INFERENCE TIME (AIT, MS) ACROSS DIFFERENT METHODS. THE BEST RESULT IS HIGHLIGHTED IN BOLD, AND THE SECOND-BEST RESULT IS UNDERLINED.

Method	mAP5°	Params (M)	FLOPs (G)	ART (ms)	AIT (ms)
CLNet [16]	54.05	<b>0.95</b>	<b>1.92</b>	<b>181.87</b>	<b>4.13</b>
MS <sup>2</sup> DGNet [28]	49.13	2.53	5.32	396.19	9.35
NCMNet [17]	63.52	4.49	8.72	855.14	15.58
GCTNet [57]	63.80	4.09	10.33	428.80	5.86
BCLNet [56]	66.08	6.65	10.93	687.15	10.53
MatchMamba [20]	<u>67.60</u>	2.08	5.15	383.31	5.03
SFMambaNet(ours)	<b>73.83</b>	<u>2.01</u>	<u>5.01</u>	<u>370.42</u>	<u>4.80</u>

Mamba further improves point-level context modeling, while DP and BiCSM introduce hierarchical cluster structure and regional spatial Mamba aggregation, yielding additional gains. The complete LSGA with MSI achieves the best result, reaching 64.88% mAP5° and 83.48% mAP20°, demonstrating that cross-scale interaction between point-level and cluster-level features is necessary to fully exploit the spectral-geometric representation.

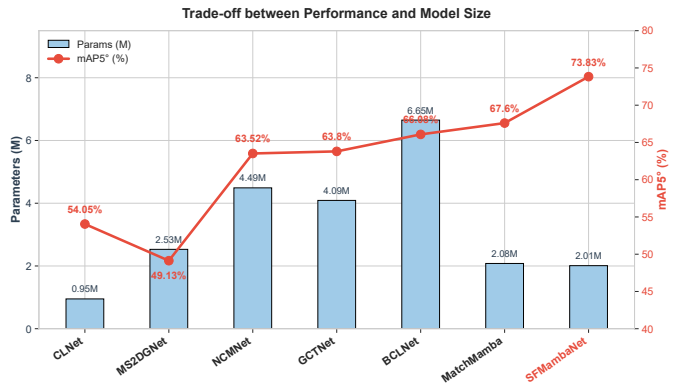


Fig. 8. Visualization of the trade-off between estimation accuracy (mAP5° on the unknown split) and model parameter size across different methods on outdoor YFCC100M with SIFT features. The bar chart (left y-axis) represents the parameter count in millions, while the line chart (right y-axis) indicates the corresponding camera pose estimation accuracy.

**How efficient is SFMambaNet?** Beyond accuracy, we benchmark the computational efficiency of SFMambaNet on the unknown split of outdoor YFCC100M, focusing on floating-point operations (FLOPs), parameter size (Params), average runtime per epoch (ART), and average inference time (AIT). We conduct a comparative analysis against existing state-of-the-art methods, including the Transformer-based MS<sup>2</sup>DGNet [28] and BCLNet [56], alongside CLNet [16], NCMNet [17], GCTNet [57], and MatchMamba [20]. As shown in Table VII, SFMambaNet consistently ranks among the top two in the accuracy-efficiency comparison. Specifically, relative to MatchMamba [20], our method yields a 6.23% improvement in mAP5° on the unknown split while requiring fewer parameters, FLOPs, and runtime. Furthermore, compared to the recent Transformer-based BCLNet, SFMambaNet

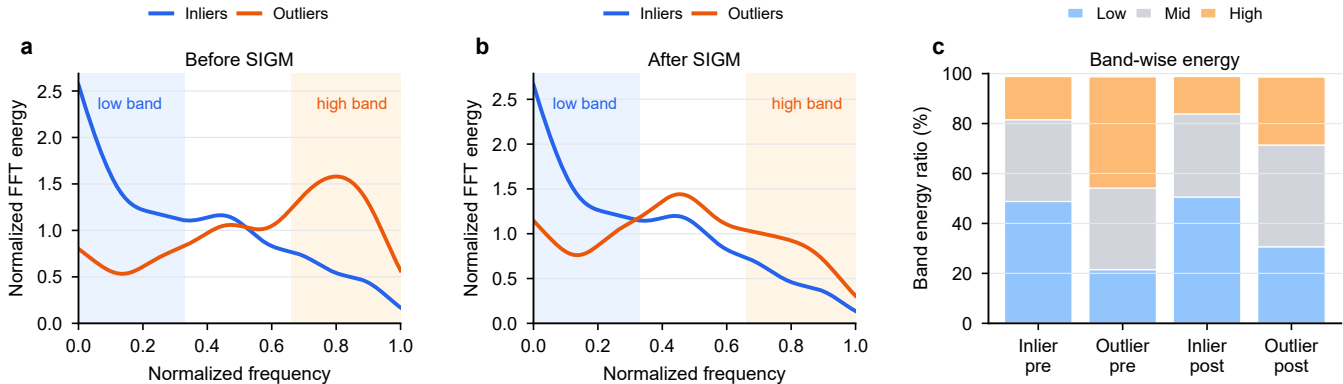


Fig. 9. Frequency-domain diagnostic of the SIGM block. (a) Normalized FFT energy distribution of inlier and outlier features before SIGM. (b) Corresponding distribution after SIGM. (c) Band-wise energy ratios in low-, mid-, and high-frequency ranges. The low- and high-frequency regions are highlighted to show how SIGM attenuates unstable high-frequency components while preserving low-frequency consensus cues.

not only delivers superior performance but also demonstrates remarkable efficiency gains, reducing the parameter count by approximately 69.77% and FLOPs by 54.16%. Correspondingly, the training and inference latencies are decreased by 46.09% and 54.42%, respectively. These results substantiate the feasibility and efficiency of replacing heavy Transformers with our frequency-domain Mamba architecture. As shown in Fig. 8, our proposed SFMambaNet strikes the optimal balance, achieving the state-of-the-art accuracy on the unknown split while preserving a highly competitive lightweight architecture.

**Does Bidirectional Mamba with Frequency Gating Mechanism Effectively Suppress the Accumulation of Inconsistent Features in the Hidden State Space?** To verify the efficacy of the bidirectional scanning strategy integrated with frequency gating, we performed comparative experiments on outdoor YFCC100M involving three distinct modes: unidirectional, random, and frequency-gated bidirectional. As shown in Table VIII, the frequency-gated bidirectional scanning consistently achieves the best performance on outdoor YFCC100M under both known and unknown splits. We attribute this to the dual perception in the spatial-frequency domain, which performs a gating mechanism in the frequency domain. This enhances a more comprehensive view and suppresses high-frequency noise, thereby reducing the propagation of inconsistent information. Conversely, random scanning yields inferior results compared to the unidirectional approach. This degradation likely stems from the disordered shuffling of correspondences with significant variances, which introduces information inconsistency. Note that to ensure a fair comparison, the number of Mamba blocks remains constant across all models, with the scanning strategy being the sole variable.

**Frequency-domain diagnostic of SIGM.** To empirically examine the spectral assumption behind our design, we apply FFT to the cluster-ordered SIGM input  $F_{ord}^{GL}$  and the SIGM output  $F^O$ , and average the normalized spectral energy over inlier and outlier correspondences on the unknown split of outdoor YFCC100M. As shown in Fig. 9, before SIGM, inliers concentrate more energy in the low-frequency band, whereas

TABLE VIII  
ABLATION STUDY OF DIFFERENT SCANNING STRATEGIES OF SFMAMBA<sub>NET</sub> ON OUTDOOR YFCC100M, REPORTING MAP5° AND MAP20° RESULTS FOR KNOWN AND UNKNOWN SCENES WITHOUT RANSAC. HERE, MAMBA, RMAMBA, AND SIGM DENOTE UNIDIRECTIONAL, RANDOM, AND FREQUENCY-GATED BIDIRECTIONAL SCANNING, RESPECTIVELY.

Components				Known		Unknown	
Baseline	Mamba	RMamba	SIGM	mAP5°	mAP20°	mAP5°	mAP20°
✓				40.37	61.11	55.97	75.21
✓	✓			50.21	69.57	63.18	81.75
✓		✓		49.20	68.99	62.50	81.46
✓			✓	<b>52.21</b>	<b>73.59</b>	<b>66.60</b>	<b>83.89</b>

outliers exhibit a stronger high-frequency component, supporting the smooth-consensus intuition used in our motivation. After SIGM, the high-frequency energy of outliers is markedly attenuated while the dominant low-frequency energy of inliers is largely preserved, and the band-wise statistics show a clearer low/high-frequency separation. These observations indicate that the frequency gate acts as a spectral regularizer rather than a rigid hand-crafted filter, reducing unstable hidden-state components without suppressing the low-frequency geometric consensus required for pose estimation.

## V. CONCLUSION

In this paper, we propose SFMambaNet, a novel framework that pioneers the integration of frequency domain perception into the selective state space model for robust correspondence pruning. Specifically, the proposed Local Spectral-Geometric Attention (LSGA) block incorporates spectral positional encoding features to capture subtle geometric consistencies often overlooked by standard GNNs, while enhancing local context representation. Furthermore, the Spectral-Integrated Global Mamba (SIGM) block innovatively embeds a frequency gating mechanism within global context modeling. This design enables the network to selectively suppress high-frequency noise while establishing reliable long-range dependencies, effectively cleansing inconsistent features in the hidden state

space during information propagation to enhance global context representation. Extensive experiments demonstrate that SFMambaNet consistently outperforms various state-of-the-art networks in correspondence pruning tasks and exhibits strong generalization ability.

## REFERENCES

- [1] T. Sattler, W. Maddern, C. Toft, A. Torii, L. Hammarstrand, E. Stenborg, D. Safari, M. Okutomi, M. Pollefeys, J. Sivic *et al.*, “Benchmarking 6dof outdoor visual localization in changing conditions,” in *Proc. IEEE/CVF Conf. Comput. Vis. Pattern Recognit. (CVPR)*, 2018, pp. 8601–8610.
- [2] J. Ma, H. Zhou, J. Zhao, Y. Gao, J. Jiang, and J. Tian, “Robust feature matching for remote sensing image registration via locally linear transforming,” *IEEE Trans. Geosci. Remote Sens.*, vol. 53, no. 12, pp. 6469–6481, 2015.
- [3] F. Zhuang, Y. Liu, X. Li, J. Zhou, R. Chen, L. Wei, C. Yang, and J. Ma, “Multi-granularity consensus network for remote sensing image correspondence pruning,” *ISPRS J. Photogramm. Remote Sens.*, vol. 219, pp. 38–51, 2025.
- [4] R. Mur-Artal, J. M. M. Montiel, and J. D. Tardos, “Orb-slam: A versatile and accurate monocular slam system,” *IEEE Trans. Robot.*, vol. 31, no. 5, pp. 1147–1163, 2015.
- [5] J. L. Schonberger and J.-M. Frahm, “Structure-from-motion revisited,” in *Proc. IEEE/CVF Conf. Comput. Vis. Pattern Recognit. (CVPR)*, 2016, pp. 4104–4113.
- [6] J. Wang, X. Liu, L. Dai, J. Ma, L. Wei, C. Yang, and R. Chen, “Pgn-net: Progressive guidance network via robust contextual embedding for efficient point cloud registration,” *IEEE Trans. Geosci. Remote Sens.*, vol. 61, pp. 1–12, 2023.
- [7] D. G. Lowe, “Distinctive image features from scale-invariant keypoints,” *Int. J. Comput. Vis.*, vol. 60, pp. 91–110, 2004.
- [8] D. DeTone, T. Malisiewicz, and A. Rabinovich, “Superpoint: Self-supervised interest point detection and description,” in *Proc. IEEE/CVF Conf. Comput. Vis. Pattern Recognit. Workshops (CVPRW)*, 2018, pp. 224–236.
- [9] M. A. Fischler and R. C. Bolles, “Random sample consensus: a paradigm for model fitting with applications to image analysis and automated cartography,” *Commun. ACM*, vol. 24, no. 6, pp. 381–395, 1981.
- [10] P. H. Torr and A. Zisserman, “Mlesac: A new robust estimator with application to estimating image geometry,” *Comput. Vis. Image Understand.*, vol. 78, no. 1, pp. 138–156, 2000.
- [11] R. Raguram, O. Chum, M. Pollefeys, J. Matas, and J.-M. Frahm, “Usac: A universal framework for random sample consensus,” *IEEE Trans. Pattern Anal. Mach. Intell.*, vol. 35, no. 8, pp. 2022–2038, 2012.
- [12] K. M. Yi, E. Trulls, Y. Ono, V. Lepetit, M. Salzmann, and P. Fua, “Learning to find good correspondences,” in *Proc. IEEE/CVF Conf. Comput. Vis. Pattern Recognit. (CVPR)*, 2018, pp. 2666–2674.
- [13] T. Liao, X. Zhang, L. Zhao, T. Wang, and G. Xiao, “Vsformer: Visual-spatial fusion transformer for correspondence pruning,” in *Proc. AAAI Conf. Artif. Intell.*, vol. 38, no. 4, 2024, pp. 3369–3377.
- [14] Y. Liu, Y. Li, and S. Zhao, “Transmatch: Transformer-based correspondence pruning via local and global consensus,” *Pattern Recognit.*, vol. 159, p. 111120, 2025.
- [15] C. Zhao, Z. Cao, C. Li, X. Li, and J. Yang, “Nm-net: Mining reliable neighbors for robust feature correspondences,” in *Proc. IEEE/CVF Conf. Comput. Vis. Pattern Recognit. (CVPR)*, 2019, pp. 215–224.
- [16] C. Zhao, Y. Ge, F. Zhu, R. Zhao, H. Li, and M. Salzmann, “Progressive correspondence pruning by consensus learning,” in *Proc. IEEE/CVF Int. Conf. Comput. Vis. (ICCV)*, 2021, pp. 6464–6473.
- [17] X. Liu and J. Yang, “Progressive neighbor consistency mining for correspondence pruning,” in *Proc. IEEE/CVF Conf. Comput. Vis. Pattern Recognit. (CVPR)*, 2023, pp. 9527–9537.
- [18] A. Gu and T. Dao, “Mamba: Linear-time sequence modeling with selective state spaces,” arXiv preprint arXiv:2312.00752, 2023.
- [19] A. Gu, K. Goel, and C. Ré, “Efficiently modeling long sequences with structured state spaces,” in *Proc. Int. Conf. Learn. Represent.*, 2022.
- [20] Y. Wu, X. Li, H. Chen, C. Yang, L. Wei, and R. Chen, “Matchmamba: Correspondence pruning via selective state space model,” *IEEE Trans. Circuits Syst. Video Technol.*, 2025.
- [21] J. Zhang, D. Sun, Z. Luo, A. Yao, L. Zhou, T. Shen, Y. Chen, L. Quan, and H. Liao, “Learning two-view correspondences and geometry using order-aware network,” in *Proc. IEEE/CVF Int. Conf. Comput. Vis. (ICCV)*, 2019, pp. 5845–5854.
- [22] A. Fan, X. Jiang, Y. Ma, X. Mei, and J. Ma, “Smoothness-driven consensus based on compact representation for robust feature matching,” *IEEE Trans. Neural Netw. Learn. Syst.*, vol. 34, no. 8, pp. 4460–4472, 2023.
- [23] J. Bian, W.-Y. Lin, Y. Matsushita, S.-K. Yeung, T.-D. Nguyen, and M.-M. Cheng, “Gms: Grid-based motion statistics for fast, ultra-robust feature correspondence,” in *Proc. IEEE/CVF Conf. Comput. Vis. Pattern Recognit. (CVPR)*, 2017, pp. 4181–4190.
- [24] O. Chum and J. Matas, “Matching with prosac-progressive sample consensus,” in *Proc. IEEE/CVF Conf. Comput. Vis. Pattern Recognit. (CVPR)*, vol. 1. IEEE, 2005, pp. 220–226.
- [25] D. Barath, J. Matas, and J. Noskova, “Magsac: marginalizing sample consensus,” in *Proc. IEEE/CVF Conf. Comput. Vis. Pattern Recognit. (CVPR)*, 2019, pp. 10 197–10 205.
- [26] J. Ma, J. Zhao, J. Tian, A. L. Yuille, and Z. Tu, “Robust point matching via vector field consensus,” *IEEE Trans. Image Process.*, vol. 23, no. 4, pp. 1706–1721, 2014.
- [27] J. Ma, J. Zhao, J. Jiang, H. Zhou, and X. Guo, “Locality preserving matching,” *Int. J. Comput. Vis.*, vol. 127, pp. 512–531, 2019.
- [28] L. Dai, Y. Liu, J. Ma, L. Wei, T. Lai, C. Yang, and R. Chen, “Ms2dg-net: Progressive correspondence learning via multiple sparse semantics dynamic graph,” in *Proc. IEEE/CVF Conf. Comput. Vis. Pattern Recognit. (CVPR)*, 2022, pp. 8973–8982.
- [29] M. Shen, G. Xiao, C. Yang, J. Guo, and L. Zhu, “Clg-net: Rethinking local and global perception in lightweight two-view correspondence learning,” *IEEE Trans. Circuits Syst. Video Technol.*, 2024.
- [30] S. Lin, M. Lo, H. Chen, Y. Liang, and Q. Wu, “Mgca-net: Multi-graph contextual attention network for two-view correspondence learning,” in *Proc. Int. Joint Conf. Artif. Intell.*, ser. IJCAI-2025. International Joint Conferences on Artificial Intelligence Organization, Sep. 2025, p. 1539–1547.
- [31] L. Zhu, B. Liao, Q. Zhang, X. Wang, W. Liu, and X. Wang, “Vision mamba: Efficient visual representation learning with bidirectional state space model,” in *Proc. Int. Conf. Mach. Learn.*, 2024.
- [32] Y. Liu, Y. Tian, Y. Zhao, H. Yu, L. Xie, Y. Wang, Q. Ye, J. Jiao, and Y. Liu, “Vmamba: Visual state space model,” in *Proc. Adv. Neural Inf. Process. Syst.*, 2024.
- [33] A. Dosovitskiy, “An image is worth 16x16 words: Transformers for image recognition at scale,” in *Proc. Int. Conf. Learn. Represent.*, 2021.
- [34] D. Liang, X. Zhou, W. Xu, X. Zhu, Z. Zou, X. Ye, X. Tan, and X. Bai, “Pointmamba: A simple state space model for point cloud analysis,” arXiv preprint arXiv:2402.10739, 2024.
- [35] H. Sun, L. Lv, P. Zhang, T. Tang, F. Tian, W. Sun, and H. Lu, “Spatial-frequency enhanced mamba for multi-modal image fusion,” *IEEE Trans. Image Process.*, vol. 34, pp. 7684–7696, 2025.
- [36] M. Deng, S. Sun, Z. Li, X. Hu, and X. Wu, “Fmnet: Frequency-assisted mamba-like linear attention network for camouflaged object detection,” arXiv preprint arXiv:2503.11030, 2025.
- [37] Y. Xia and J. Ma, “Grid-guided sparse laplacian consensus for robust feature matching,” *IEEE Trans. Image Process.*, 2025.
- [38] M. Tancik, P. Srinivasan, B. Mildenhall, S. Fridovich-Keil, N. Raghavan, U. Singhal, R. Ramamoorthi, J. Barron, and R. Ng, “Fourier features let networks learn high frequency functions in low dimensional domains,” *Proc. Adv. Neural Inf. Process. Syst.*, vol. 33, pp. 7537–7547, 2020.
- [39] Z. Ying, J. You, C. Morris, X. Ren, W. Hamilton, and J. Leskovec, “Hierarchical graph representation learning with differentiable pooling,” *Proc. Adv. Neural Inf. Process. Syst.*, vol. 31, 2018.
- [40] C. Wang, O. Tsepa, J. Ma, and B. Wang, “Graph-mamba: Towards long-range graph sequence modeling with selective state spaces,” arXiv preprint arXiv:2402.00789, 2024.
- [41] A. Behrouz and F. Hashemi, “Graph mamba: Towards learning on graphs with state space models,” in *Proc. ACM SIGKDD Conf. Knowl. Discovery Data Mining (KDD)*, 2024, pp. 119–130.
- [42] Y. Rao, W. Zhao, Z. Zhu, J. Lu, and J. Zhou, “Global filter networks for image classification,” *Proc. Adv. Neural Inf. Process. Syst.*, vol. 34, pp. 980–993, 2021.
- [43] J. Guibas, M. Mardani, Z. Li, A. Tao, A. Anandkumar, and B. Catanzaro, “Efficient token mixing for transformers via adaptive fourier neural operators,” in *Proc. Int. Conf. Learn. Represent.*, 2021.
- [44] D. P. Kingma, “Adam: A method for stochastic optimization,” arXiv preprint arXiv:1412.6980, 2014.
- [45] B. Thomee, D. A. Shamma, G. Friedland, B. Elizalde, K. Ni, D. Poland, D. Borth, and L.-J. Li, “Yfcc100m: The new data in multimedia research,” *Commun. ACM*, vol. 59, no. 2, pp. 64–73, 2016.
- [46] J. Xiao, A. Owens, and A. Torralba, “Sun3d: A database of big spaces reconstructed using sfm and object labels,” in *Proc. IEEE/CVF Int. Conf. Comput. Vis. (ICCV)*, 2013, pp. 1625–1632.

- [47] A. Dai, A. X. Chang, M. Savva, M. Halber, T. Funkhouser, and M. Niessner, "Scannet: Richly-annotated 3d reconstructions of indoor scenes," in *Proc. IEEE/CVF Conf. Comput. Vis. Pattern Recognit. (CVPR)*, July 2017.
- [48] C. R. Qi, L. Yi, H. Su, and L. J. Guibas, "Pointnet++: Deep hierarchical feature learning on point sets in a metric space," *Proc. Adv. Neural Inf. Process. Syst.*, vol. 30, 2017.
- [49] P.-E. Sarlin, D. DeTone, T. Malisiewicz, and A. Rabinovich, "Super-glue: Learning feature matching with graph neural networks," in *Proc. IEEE/CVF Conf. Comput. Vis. Pattern Recognit. (CVPR)*, 2020, pp. 4938–4947.
- [50] W. Sun, W. Jiang, E. Trulls, A. Tagliasacchi, and K. M. Yi, "Acne: Attentive context normalization for robust permutation-equivariant learning," in *Proc. IEEE/CVF Conf. Comput. Vis. Pattern Recognit. (CVPR)*, 2020, pp. 11 286–11 295.
- [51] Z. Zhong, G. Xiao, L. Zheng, Y. Lu, and J. Ma, "T-net: Effective permutation-equivariant network for two-view correspondence learning," in *Proc. IEEE/CVF Int. Conf. Comput. Vis. (ICCV)*, 2021, pp. 1950–1959.
- [52] Z. Li, S. Zhang, and J. Ma, "U-match: Two-view correspondence learning with hierarchy-aware local context aggregation," in *Proc. Int. Joint Conf. Artif. Intell.*, 2023, pp. 1169–1176.
- [53] X. Liu, G. Xiao, R. Chen, and J. Ma, "Pgfnet: Preference-guided filtering network for two-view correspondence learning," *IEEE Trans. Image Process.*, vol. 32, pp. 1367–1378, 2023.
- [54] L. Dai, X. Du, H. Zhang, and J. Tang, "Mgnet: Learning correspondences via multiple graphs," in *Proc. AAAI Conf. Artif. Intell.*, vol. 38, no. 4, 2024, pp. 3945–3953.
- [55] S. Lin, X. Chen, G. Xiao, H. Wang, F. Huang, and J. Weng, "Multi-stage network with geometric semantic attention for two-view correspondence learning," *IEEE Trans. Image Process.*, 2024.
- [56] X. Miao, G. Xiao, S. Wang, and J. Yu, "Bclnet: Bilateral consensus learning for two-view correspondence pruning," in *Proc. AAAI Conf. Artif. Intell.*, vol. 38, no. 5, 2024, pp. 4225–4232.
- [57] J. Guo, G. Xiao, S. Wang, and J. Yu, "Graph context transformation learning for progressive correspondence pruning," in *Proc. AAAI Conf. Artif. Intell.*, vol. 38, no. 3, 2024, pp. 1968–1975.
- [58] V. Balntas, K. Lenc, A. Vedaldi, and K. Mikolajczyk, "Hpatches: A benchmark and evaluation of handcrafted and learned local descriptors," in *Proc. IEEE/CVF Conf. Comput. Vis. Pattern Recognit. (CVPR)*, 2017, pp. 5173–5182.

## BIOGRAPHY SECTION



**Zhihua Wang** is currently an undergraduate student in Computer Science and Technology at the School of Optical-Electrical and Computer Engineering, University of Shanghai for Science and Technology, China. His research interests include computer vision, deep learning, feature matching, and large language model security.



**Yanping Li** received the M.S. degree in Computer Science and Technology from Hohai University, Nanjing, China, in 2020, and the D.Eng. degree in Electronic Information Engineering from Tongji University, Shanghai, in 2024. She is currently a postdoctoral fellow at the Institute of Artificial Intelligence, Shanghai Jiao Tong University, co-advised by Professor Xiaokang Yang. Her research interests include computer vision, person re-identification, and image matching. She has published several articles in IEEE Transactions on Image Processing, Pattern Recognition, Neurocomputing, IEEE Geoscience and Remote Sensing Letters, and ACM MM.



**Yizhang Liu** received the B.S. degree in electronic and information engineering and the master's degree in computer science and technology from Fujian Agriculture and Forestry University, Fuzhou, China, in 2017 and 2020, respectively, and the Eng.D. degree in electronic information engineering from Tongji University, Shanghai, in 2024. He is a Lecturer with the College of Computer and Data Science, Fuzhou University, Fuzhou. He has published more than ten papers in IEEE Transactions on Image Processing, IEEE Transactions on Multimedia, IEEE Transactions on Geoscience and Remote Sensing, IEEE Transactions on Circuits and Systems for Video Technology, Pattern Recognition, ISPRS Journal of Photogrammetry and Remote Sensing, Knowledge-based Systems, Neurocomputing, IEEE Geoscience and Remote Sensing Letters, and ACM MM.

Pattern Recognition, Neurocomputing, IEEE Geoscience and Remote Sensing Letters, and ACM MM.